



# Hexagonal $Zr_3X$ ( $X = Al, Ga, In$ ) Metals: High Dynamic Stability, Nodal Loop, and Perfect Nodal Surface States

Heju Xu, Hailong Xi and Yong-Chun Gao\*

College of Science, North China University of Science and Technology, Tangshan, China

## OPEN ACCESS

### Edited by:

Zhenxiang Cheng,  
University of Wollongong, Australia

### Reviewed by:

Songtao Li,  
North China Electric Power  
University, China  
Yajiu Zhang,  
Guangzhou University, China

### \*Correspondence:

Yong-Chun Gao  
gaoyc1963@ncst.edu.cn

### Specialty section:

This article was submitted to  
Theoretical and Computational  
Chemistry,  
a section of the journal  
Frontiers in Chemistry

**Received:** 20 September 2020

**Accepted:** 30 September 2020

**Published:** 19 November 2020

### Citation:

Xu H, Xi H and Gao Y-C (2020)  
Hexagonal  $Zr_3X$  ( $X = Al, Ga, In$ )  
Metals: High Dynamic Stability, Nodal  
Loop, and Perfect Nodal Surface  
States. *Front. Chem.* 8:608398.  
doi: 10.3389/fchem.2020.608398

In recent years, topological semimetals/metals, including nodal point, nodal line, and nodal surface semimetals/metals, have been studied extensively because of their potential applications in spintronics and quantum computers. In this study, we predict a family of materials,  $Zr_3X$  ( $X = Al, Ga, In$ ), hosting the nodal loop and nodal surface states in the absence of spin-orbit coupling. Remarkably, the energy variation of the nodal loop and nodal surface states in  $Zr_3X$  are very small, and these topological signatures lie very close to the Fermi level. When the effect of spin-orbit coupling is considered, the nodal loop and nodal surface states exhibit small energy gaps (<25 and 35 meV, respectively) that are suitable observables that reflect the spin-orbit coupling response of these topological signatures and can be detected in experiments. Moreover, these compounds are dynamically stable, and they consequently form potential material platforms to study nodal loop and nodal surface semimetals.

**Keywords:** nodal loop states, nodal surface states, first-principles, electronic structures, spin-orbit-coupling

## INTRODUCTION

The exploration of non-trivial topologies in crystalline solids has attracted significant attention from chemists, physicists, and material scientists (Kong and Cui, 2011; Cava et al., 2013; Banik et al., 2018; Zhang et al., 2018a; Tang et al., 2019). The main features of these topological solids are enclosed in their electronic-band structures. Initially, research was conducted in the context of the insulating state (Zhang et al., 2011; Li et al., 2012; Peng et al., 2012; Rasche et al., 2013; Wang et al., 2013; Kambe et al., 2014; Chang et al., 2015; Walsh et al., 2017; Barton et al., 2019; Zeugner et al., 2019), and the concept of band topology has now been extended to the metallic and semi-metallic states (Bradlyn et al., 2017; Bernevig et al., 2018; Schoop et al., 2018; Zhou et al., 2018; Gao et al., 2019; Hu et al., 2019; Klemenz et al., 2020; Wang et al., 2020b,c; Zhao Z. et al., 2020) as well.

The dimensionality of band-crossings is a criterion used to classify topological semimetals/metals. The most famous topological semimetals/metals with zero-dimensional band-crossings, i.e., zero-dimensional nodal points, are Dirac semimetals/metals (Chen et al., 2015, 2020; Bradlyn et al., 2017; Zhong et al., 2017; Jing and Heine, 2018; Liu et al., 2018b; Zhang et al., 2018b; Khoury et al., 2019; Wang et al., 2020f; Xu et al., 2020) and Weyl semimetals/metals

(Peng et al., 2016; Lin et al., 2017; Fu et al., 2018; Zhang et al., 2018c; Zhou et al., 2019; Gupta et al., 2020; Jia et al., 2020; Liu et al., 2020; Meng L. et al., 2020; Zhao B. et al., 2020). We selected Weyl semimetals/metals as examples here because there exists a band-crossing of the valence band and conduction band at an isolated nodal point in the momentum space of these solids. Particularly, around this isolated nodal point, the quasiparticle acts similarly to the behavior of Weyl fermions, which are particles of considerable interest in high-energy physics. We summarize some recent studies on Weyl materials as follows: (i) Zhao and Ma (2020) stated that hexagonal MnO ferromagnet is a magnetic Weyl semimetal with spin-gapless state; (ii) Meng W. et al. (2020b) predicted that HfCuP compound is a newly designed Weyl semimetal with different types of Weyl nodes; and (iii) Jia et al. (2020) reported that the  $VI_3$  monolayer hosts a Weyl fermion and 100% spin-polarization. Furthermore, under the protection from certain crystalline symmetries, two Weyl points of opposite chirality can be stable at the same point, forming a Dirac point.

In the case of three-dimensional materials, besides the zero-dimensional nodal point metals/semimetals, in principle, there should exist one-dimensional and two-dimensional band-crossing metals/semimetals as well. For three-dimensional materials with one-dimensional band-crossings, some members, named as nodal line/loop semimetal/metals, have garnered considerable attention owing to their rich properties. Based on the shape of the nodal lines, they may host various forms, such as nodal link (Yan et al., 2017), nodal chains (Bzdušek et al., 2016), nodal boxes (Sheng et al., 2017), nodal ring (Wang et al., 2020d), nodal knot (Bi et al., 2017), and nodal net (Feng et al., 2018; Wang et al., 2018). So far, numerous types of

nodal-line semimetals/metals have been predicted (He et al., 2019, 2020; Jin et al., 2019a,b, 2020a,c; Zhang et al., 2019; Meng W. et al., 2020a; Wang et al., 2020a,e; Zhou et al., 2020), and it is assumed that the node-line states have interesting characteristics in terms of their electronic, transport, and magnetic properties.

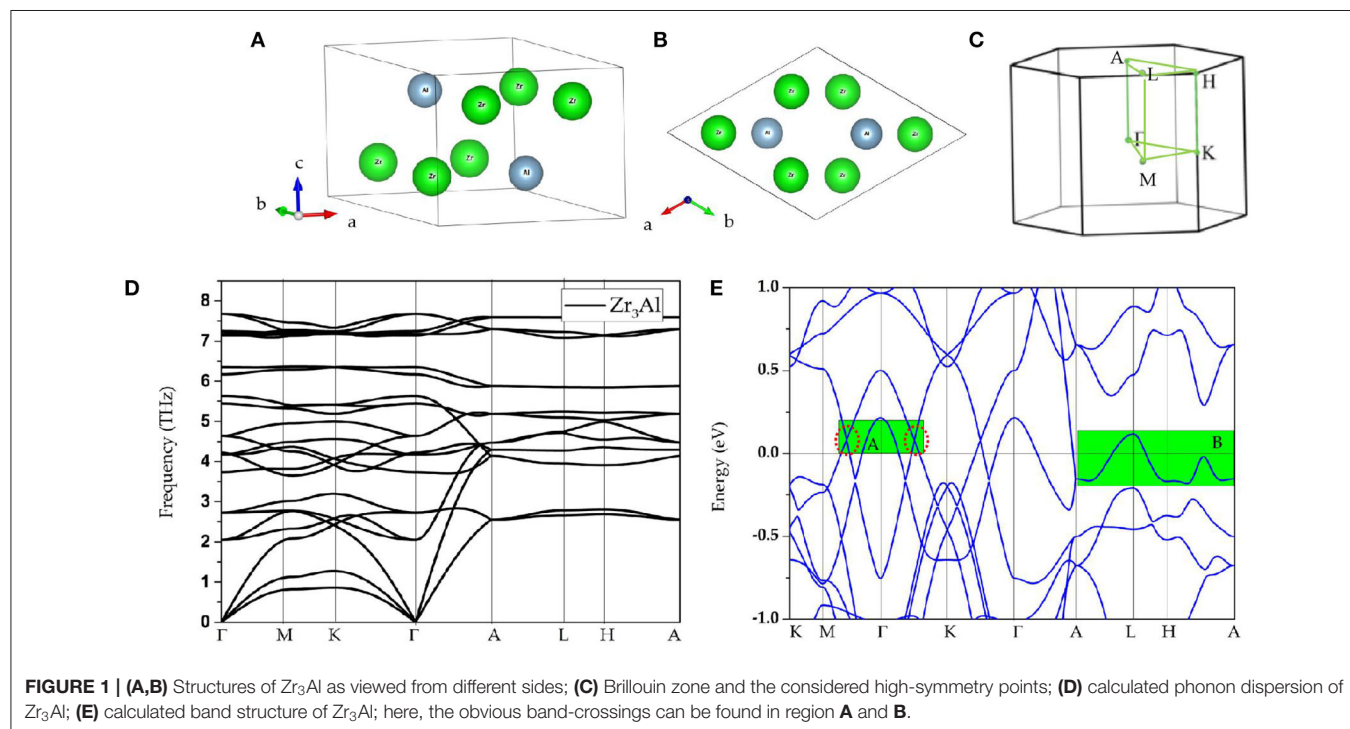
Zhong et al. (2016) had first observed topological semimetals/metals with two-dimensional band-crossings, i.e., nodal surface states. However, investigations into nodal surface semimetals/metals are very rare (Wu et al., 2018), and the energy variation of the nodal surface state is great.

If one material hosts two or more types of band-crossings, it can be considered a good platform to investigate the relationship among different topological signatures. Very recently, tetragonal PtO was proposed by Li et al. (2020b) as an effective material to study the one-dimensional nodal line and zero-dimensional nodal point states. Furthermore, Li and Xia (2020) predicted that cubic HfN is a topological material that co-exhibits nodal line and nodal loop states.

Motivated by the above-mentioned information and based on the first principles, we report a new family of topological materials,  $Zr_3X$  ( $X = Al, Ga, In$ ) with one-dimensional nodal loop and two-dimensional nodal surface states. The progress in

**TABLE 1** | Optimized lattice constants for  $Zr_3X$  compounds.

| Compounds | a (Å) | b (Å) | c (Å) |
|-----------|-------|-------|-------|
| $Zr_3Al$  | 6.202 | 6.202 | 5.371 |
| $Zr_3Ga$  | 6.166 | 6.166 | 5.052 |
| $Zr_3In$  | 6.325 | 6.325 | 5.221 |



the field of nodal line/surface states, including the conceptual development, the character and classification of these nodal structures, and the material realization, can be found in Wang et al. (2019). Moreover, the dynamical stable as well as the effect of spin-orbit coupling on the electronic structures of these materials are discussed in detail.

## MATERIALS

In this study, we have focused on the hexagonal type  $Zr_3X$  ( $X = Al, Ga, In$ ). As an example, the primitive cell structure of hexagonal  $P6_3/mmc$  type  $Zr_3Al$  from different sides are shown in **Figures 1A,B**. From the figures, it is evident that  $Zr_3X$  has eight atoms, namely, two  $X$  atoms and six  $Zr$  atoms. The structures of  $Zr_3X$  have been totally relaxed with the help of first principles. The equilibrium lattice parameters of  $Zr_3X$  ( $X = Al, Ga, In$ ) have been computed via minimizing the crystal total energy calculated for different values of lattice constant by means of Murnaghan's equation of state (EOS) (Murnaghan, 1944). The achieved lattice constants for these compounds are shown in **Table 1**.

Based on the Brillouin zone and considered high-symmetry points  $\Gamma$ -M-K- $\Gamma$ -A-L-H-A (as shown in **Figure 1C**), dynamic stability was examined for these three compounds according to the calculated phonon dispersions, and the results are given in **Figures 1D, 2A,B**, respectively. These  $Zr_3X$  compounds are

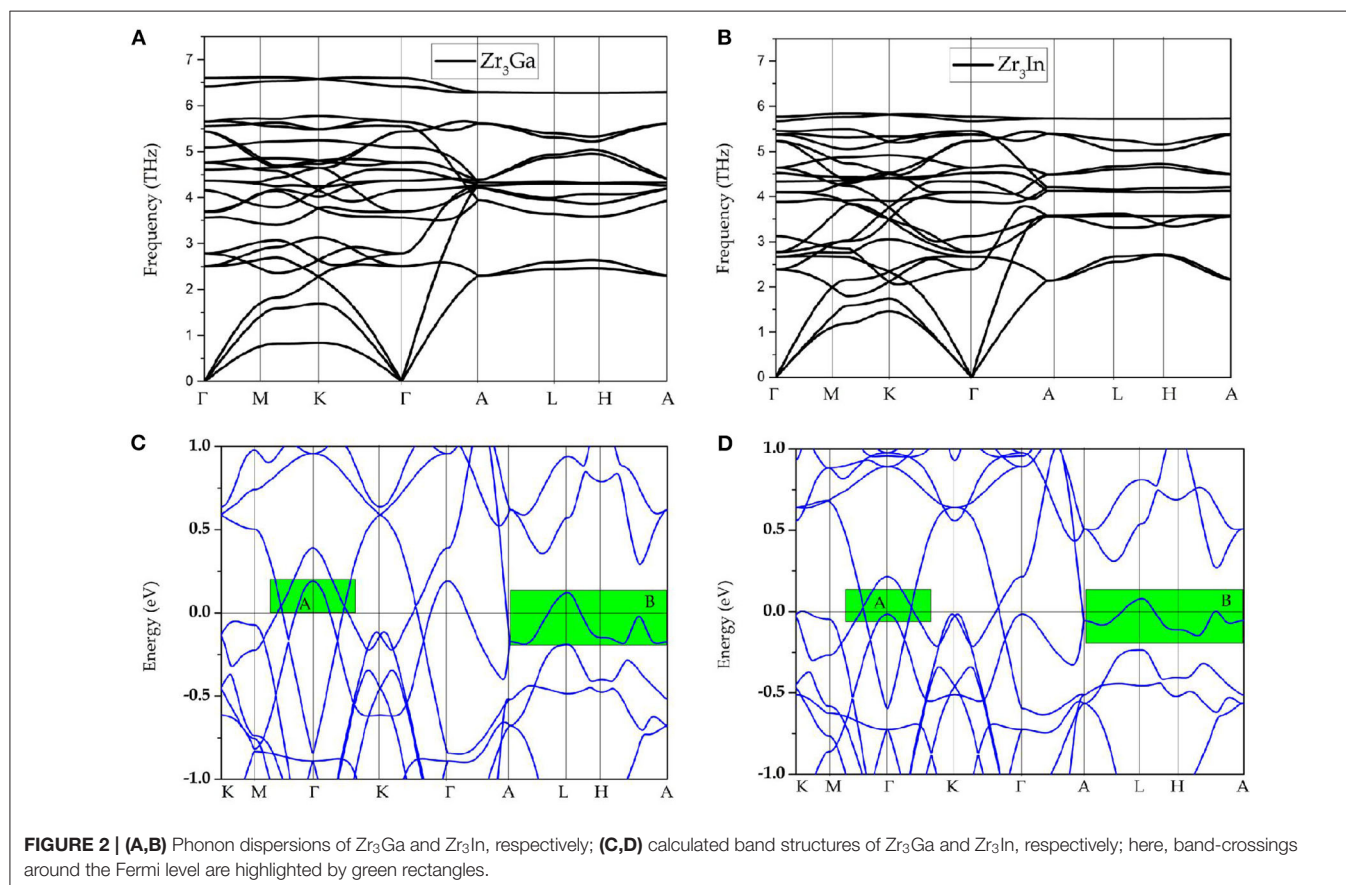
obviously dynamically stable due to the absence of the imaginary frequency (Han et al., 2019; Wu et al., 2019; Li et al., 2020a). These materials are therefore proposed to be experimental platforms to study topological semimetals/metals.

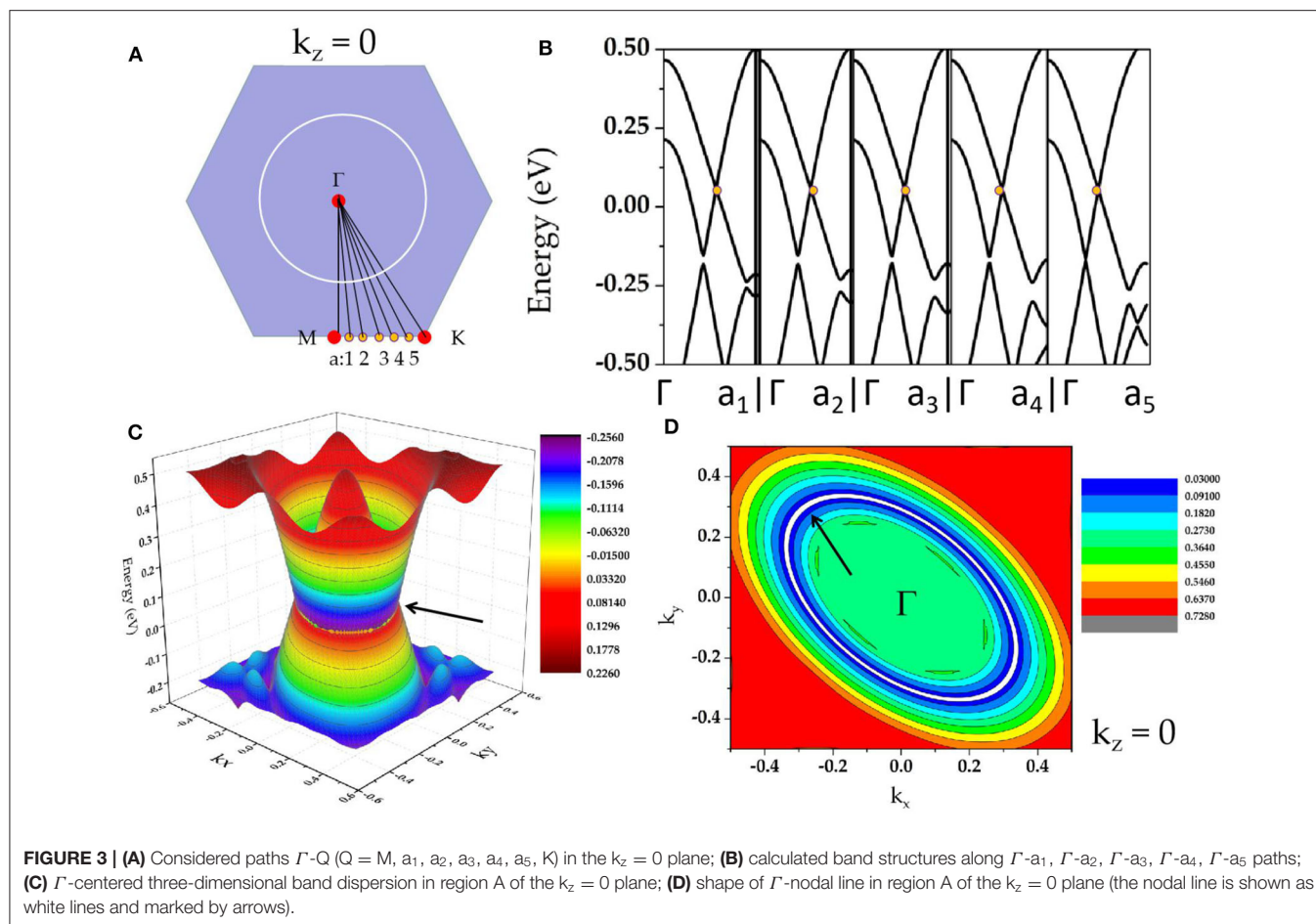
## COMPUTATIONAL METHODS

In this study, calculations have been carried out using the Vienna ab initio simulation package (VASP) (Kresse and Furthmüller, 1996) based on the first-principles density functional theory (DFT), and the generalized gradient approximation (GGA) (Perdew et al., 1996) of Perdew–Burke–Ernzerhof (PBE) (Perdew et al., 1998) functional is adopted for the exchange–correlation potential. During the calculations, the cutoff energy is set as 600 eV, and the Brillouin zone is sampled by the Monkhorst–Pack  $k$ -mesh with a size of  $6 \times 6 \times 6$ . Furthermore, we set the energy/force convergence criteria as  $10^{-6}$  eV/ $10^{-3}$  eV.

## RESULTS AND DISCUSSION

Observing the calculated band structure of  $Zr_3Al$  in **Figure 1E**, we find that  $Zr_3Al$  is a metal in which the bands and the Fermi level overlap. In addition to the metallic property, we find that there are several band-crossings near the Fermi level. These band-crossings are mainly located in two regions, named





as region A and region B, which have been highlighted by green backgrounds. Similar properties are observed in  $Zr_3Ga$  and  $Zr_3In$ , as shown in **Figures 2C,D**, respectively.

In **Figures 1E, 2C,D**, one may notice that the band structures for these  $Zr_3X$  compounds are approximately the same; hence, in the following discussion,  $Zr_3Al$  was selected as an example with which to study the band topology of  $Zr_3X$  compounds. As an example, the band structural of  $Zr_3Al$  via GGA+U ( $U = 4$  eV for Zr-d orbitals) is given in **Supplementary Figure 1**. One can find that the band topology of  $Zr_3Al$  is still kept under GGA+U method.

In **Figure 1E**, we find that the band-crossings in region A and region B are quite close to the Fermi level. Specifically, the band-crossings in region A are along M- $\Gamma$ -K paths, and the band-crossings in region B are along A-L-H-A paths. These band-crossings in both the regions may thus dominate the main features of  $Zr_3Al$ .

As shown in **Supplementary Figure 1**, in region A, we observe two obvious band-crossings; one is along M- $\Gamma$ , and the other one is along  $\Gamma$ -K.  $Zr_3Al$  is a system with inversion  $P$  and time-reversal  $T$  symmetries; thus, the two band-crossings along M- $\Gamma$ -K paths cannot be isolated points (Xu et al., 2017; Fu et al., 2019) on the plane  $k_z = 0$ . To determine that the two band-crossings in region A belong to a nodal loop on the plane  $k_z = 0$ , we

selected  $\Gamma$ - $a_1$ ,  $\Gamma$ - $a_2$ ,  $\Gamma$ - $a_3$ ,  $\Gamma$ - $a_4$ , and  $\Gamma$ - $a_5$  paths (see **Figure 3A**) to further calculate the band structures of  $Zr_3Al$  ( $a_1$ ,  $a_2$ ,  $a_3$ ,  $a_4$ , and  $a_5$  are equally spaced between M and K). The calculated band structures are shown in **Figure 3B**, and we find that band-crossings (marked as yellow circles) appear along  $\Gamma$ - $a_1$ ,  $\Gamma$ - $a_2$ ,  $\Gamma$ - $a_3$ ,  $\Gamma$ - $a_4$ , and  $\Gamma$ - $a_5$  paths, implying that a nodal loop should occur on the plane  $k_z = 0$ . The  $\Gamma$ -centered three-dimensional band dispersion in region A of the  $k_z = 0$  plane and the shape of  $\Gamma$ -nodal line in region A are shown in **Figures 3C,D**, respectively. As shown in **Figures 3B,C**, these band-crossings in region A host very little energy variation. That is,  $Zr_3X$  materials can be seen as exceedingly flat in energy, which may exhibit special properties that have exceptional applications. For example, very recently, Wang et al. (2020e) proposed that a nearly flat nodal line around the Fermi level will induce an exceptional thermoelectric power factor in the  $Nb_3GeTe_6$  monolayer. Moreover, as shown in **Figure 3B**, we find that all the band crossing points on the plane  $k_z = 0$  are type I (Liu et al., 2018a; see **Supplementary Figure 2**); this nodal line is thus type I.

In region B, one can see that there are degenerate bands along the A-L-H-A direction. This indicates that the bands in the plane  $k_z = \pi$  are doubly degenerate, reflecting a nodal surface state that appeared in the plane  $k_z = \pi$ . To further confirm that the two bands are degenerated in  $k_z = \pi$  plane,

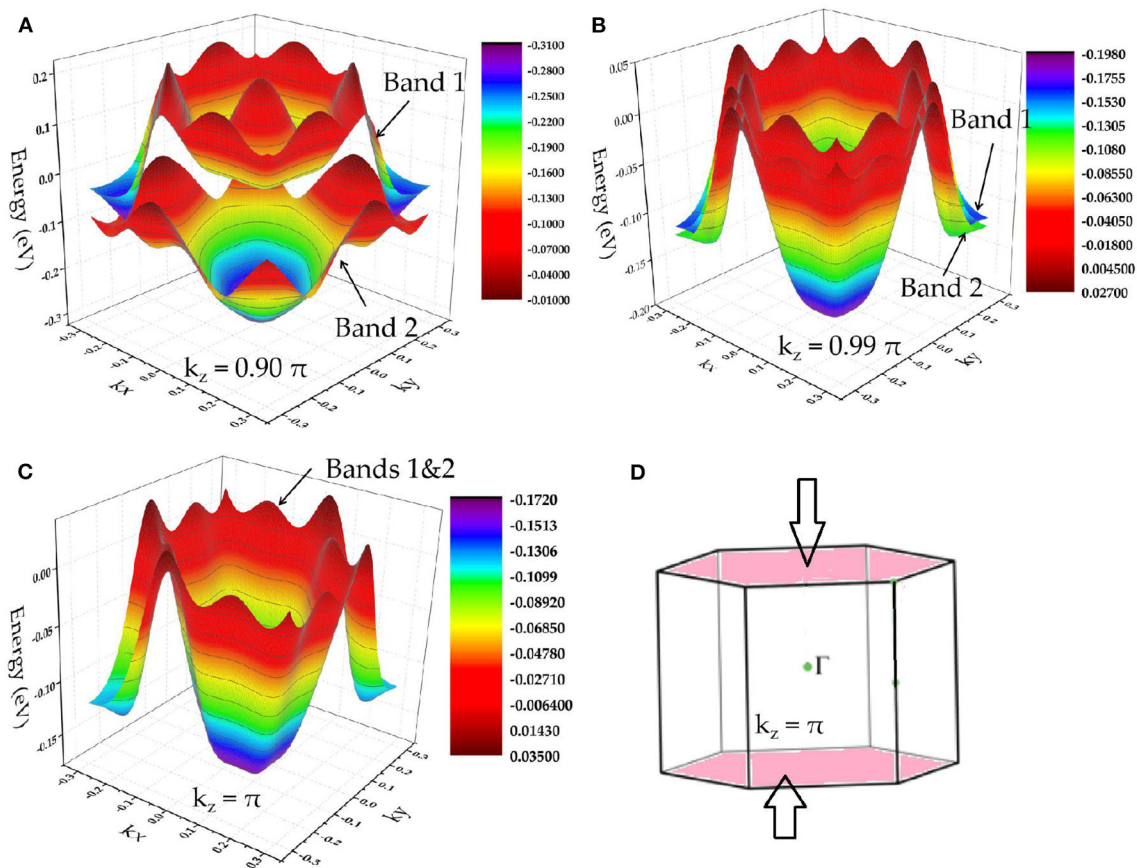


**FIGURE 4 | (A–C)** A-centered three-dimensional band dispersion in region B of the planes  $k_z = 0.90\pi$ ,  $k_z = 0.99\pi$ , and  $k_z = \pi$ , respectively; **(D)** schematic diagram indicating the nodal surface state in the  $k_z = \pi$  plane.

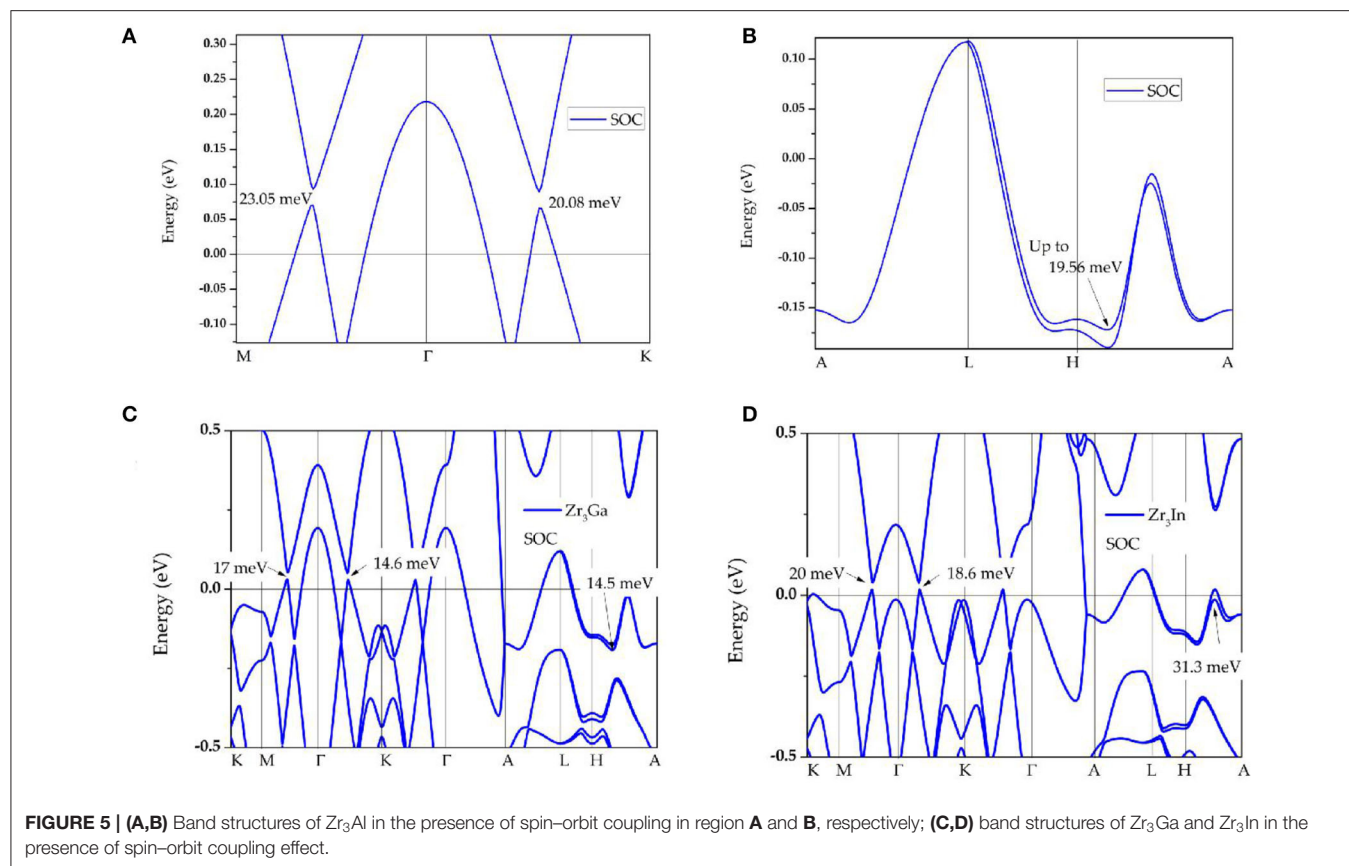
we show the A-centered three-dimensional band dispersion in region B of the planes  $k_z = 0.90\pi$ ,  $k_z = 0.99\pi$ , and  $k_z = \pi$  in **Figures 4A–C**, respectively. In **Figure 4C**, the two bands are obviously totally degenerate, leading to a new topological signature, i.e., nodal surface state, in the  $k_z = \pi$  plane (as shown in **Figure 4D**). Furthermore, as shown in **Figure 4C**, the energy variation of the nodal surface state is very small (range from  $-0.15$  to  $0.05$  eV). Similar to the situation of the nearly flat nodal line state in the  $k_z = 0$  plane, the small energy variation of the nodal surface state in the  $k_z = \pi$  plane may benefit the future experimental investigations.

Finally, we discuss the electronic-band structure in the presence of spin-orbit coupling. The corresponding calculations results are shown in **Figure 5**. We find that  $Zr_3Al$  is an excellent topological material whose band structure shows marked signatures (energy gaps) induced by the spin-orbit coupling effect (Fang et al., 2015). The spin-orbit coupling effect induces energy gaps of 23.05 and 20.08 meV (see **Figure 5A**) in region A. Furthermore, the band-crossings in region B have open energy gaps of 19.56 meV resulting from the spin-orbit coupling effect (see **Figure 5B**). The band structures of  $Zr_3Ga$  and  $Zr_3In$  with the effect of spin-orbit coupling are also exhibited

in **Figures 5C,D**, respectively. The open energy gaps observed in these topological signatures, exhibited by  $Zr_3X$  metal ( $X = Al, Ga, In$ ), are very small compared to the other well-known topological semimetals/metals (Fang et al., 2016). A detailed collection of SOC gaps of typical nodal line materials can be found in the Supplementary Information of (Jin et al., 2020b).

## SUMMARY

In summary, the topological band structures of  $Zr_3X$  ( $X = Al, Ga, In$ ) have been studied via DFT calculations in this study. Neglecting spin-orbit coupling, there is a nodal loop in the  $k_z = 0$  plane and nodal surface state in the  $k_z = \pi$  plane. The rich topological signatures are quite near to the Fermi level, which can be detected experimentally. Remarkably, the loop is nearly flat and the nodal surface features small energy variation. These above-mentioned topological signatures are not sensitive to the effect of spin-orbit coupling. Further, these compounds are proved to be dynamically stable based on the calculated phonon dispersions and host simple and clear band structures. It



is expected that these non-trivial band-crossings can be experimentally observed via angle-resolved photoemission spectroscopy (ARPES).

## DATA AVAILABILITY STATEMENT

The original contributions generated for the study are included in the article/**Supplementary Materials**, further inquiries can be directed to the corresponding author/s.

## AUTHOR CONTRIBUTIONS

HXu: investigation and writing-original draft. Y-CG: supervision. HXu and Y-CG: formal analysis. HXi: methodology.

## REFERENCES

- Banik, A., Roychowdhury, S., and Biswas, K. (2018). The journey of tin chalcogenides towards high-performance thermoelectrics and topological materials. *Chem. Commun.* 54, 6573–6590. doi: 10.1039/C8CC02230E
- Barton, A. T., Walsh, L. A., Smyth, C. M., Qin, X., Addou, R., Cormier, C., et al. (2019). Impact of etch processes on the chemistry and surface states of the topological insulator  $Bi_2Se_3$ . *ACS Appl. Mater. Interfaces* 11, 32144–32150. doi: 10.1021/acsami.9b10625

All authors contributed to the article and approved the submitted version.

## FUNDING

This study has been funded by the Science and Technology Research Project of Hebei Province Colleges and Universities (Grant No. QN2020113), and Tangshan Applied Basic Research Project (Grant No. 19130227g).

## SUPPLEMENTARY MATERIAL

The Supplementary Material for this article can be found online at: <https://www.frontiersin.org/articles/10.3389/fchem.2020.608398/full#supplementary-material>

- Bernevig, A., Weng, H., Fang, Z., and Dai, X. (2018). Recent progress in the study of topological semimetals. *J. Phys. Soc. Jpn.* 87:041001. doi: 10.7566/JPSJ.87.041001
- Bi, R., Yan, Z., Lu, L., and Wang, Z. (2017). Nodal-knot semimetals. *Phys. Rev. B* 96:201305. doi: 10.1103/PhysRevB.96.201305
- Bradlyn, B., Elcoro, L., Cano, J., Vergniory, M. G., Wang, Z., Felser, C., et al. (2017). Topological quantum chemistry. *Nature* 547, 298–305. doi: 10.1038/nature23268
- Bzdušek, T., Wu, Q., Rüegg, A., Sigrist, M., and Soluyanov, A. A. (2016). Nodal-chain metals. *Nature* 538, 75–78. doi: 10.1038/nature19099

- Cava, R. J., Ji, H., Fuccillo, M. K., Gibson, Q. D., and Hor, Y. S. (2013). Crystal structure and chemistry of topological insulators. *J. Mater. Chem. C* 1, 3176–3189. doi: 10.1039/c3tc30186a
- Chang, C. Z., Zhao, W., Kim, D. Y., Zhang, H., Assaf, B. A., Heiman, D., et al. (2015). High-precision realization of robust quantum anomalous Hall state in a hard ferromagnetic topological insulator. *Nat. Mater.* 14, 473–477. doi: 10.1038/nmat4204
- Chen, X., Chen, W., Yu, S., Xu, S., Rong, X., Huang, P., et al. (2020). Designing Dirac semimetals with a honeycomb  $Na_3Bi$ -lattice via isovalent cation substitution. *J. Mater. Chem. C* 8, 1257–1264. doi: 10.1039/C9TC05352B
- Chen, Z. G., Zhang, C., Zou, Y., Zhang, E., Yang, L., Hong, M., et al. (2015). Scalable growth of high mobility dirac semimetal  $Cd_3As_2$  microbelts. *Nano Lett.* 15, 5830–5834. doi: 10.1021/acs.nanolett.5b01885
- Fang, C., Chen, Y., Kee, H. Y., and Fu, L. (2015). Topological nodal line semimetals with and without spin-orbital coupling. *Phys. Rev. B* 92:081201. doi: 10.1103/PhysRevB.92.081201
- Fang, C., Weng, H., Dai, X., and Fang, Z. (2016). Topological nodal line semimetals. *Chin. Phys. B* 25:117106. doi: 10.1088/1674-1056/25/11/117106
- Feng, X., Yue, C., Song, Z., Wu, Q., and Wen, B. (2018). Topological Dirac nodal-net fermions in  $AlB_2$ -type  $TiB_2$  and  $ZrB_2$ . *Phys. Rev. Mater.* 2:014202. doi: 10.1103/PhysRevMaterials.2.014202
- Fu, B. B., Yi, C. J., Zhang, T. T., Caputo, M., Ma, J. Z., Gao, X., et al. (2019). Dirac nodal surfaces and nodal lines in  $ZrSiS$ . *Sci. Adv.* 5:eaau6459. doi: 10.1126/sciadv.aau6459
- Fu, C., Guin, S. N., Watzman, S. J., Li, G., Liu, E., Kumar, N., et al. (2018). Large Nernst power factor over a broad temperature range in polycrystalline Weyl semimetal NbP. *Energy Environ. Sci.* 11, 2813–2820. doi: 10.1039/C8EE02077A
- Gao, H., Venderbos, J. W., Kim, Y., and Rappe, A. M. (2019). Topological semimetals from first principles. *Ann. Rev. Mater. Res.* 49, 153–183. doi: 10.1146/annurev-matsci-070218-010049
- Gupta, U., Rajamathi, C. R., Kumar, N., Li, G., Sun, Y., Shekhar, C., et al. (2020). Effect of magnetic field on the hydrogen evolution activity using non-magnetic Weyl semimetal catalysts. *Dalton Trans.* 49, 3398–3402. doi: 10.1039/D0DT00050G
- Han, Y., Wu, M., Feng, Y., Cheng, Z., Lin, T., Yang, T., et al. (2019). Competition between cubic and tetragonal phases in all-d-metal Heusler alloys,  $X_{2-x}Mn_{1+x}V$  ( $X = Pd, Ni, Pt, Ag, Au, Ir, Co$ ;  $x = 1, 0$ ) a new potential direction of the Heusler family. *IUCrJ* 6, 465–472. doi: 10.1107/S2052252519004007
- He, T., Zhang, X., Liu, Y., Dai, X., Liu, G., Yu, Z. M., et al. (2020). Ferromagnetic hybrid nodal loop and switchable type-I and type-II Weyl fermions in two dimensions. *Phys. Rev. B* 102:075133. doi: 10.1103/PhysRevB.102.075133
- He, T., Zhang, X., Meng, W., Jin, L., Dai, X., and Liu, G. (2019). Topological nodal lines and nodal points in the antiferromagnetic material  $\beta$ - $Fe_2PO_5$ . *J. Mater. Chem. C* 7, 12657–12663. doi: 10.1039/C9TC04046C
- Hu, J., Xu, S. Y., Ni, N., and Mao, Z. (2019). Transport of topological semimetals. *Annu. Rev. Mater. Res.* 49, 207–252. doi: 10.1146/annurev-matsci-070218-010023
- Jia, T., Meng, W., Zhang, H., Liu, C., Dai, X., Zhang, X., et al. (2020). Type-II Weyl state in  $VI_3$  monolayer. *Front. Chem.* 8:722. doi: 10.3389/fchem.2020.00722
- Jin, L., Zhang, X., He, T., Meng, W., Dai, X., and Liu, G. (2019b). Topological nodal line state in superconducting  $NaAlSi$  compound. *J. Mater. Chem. C* 7, 10694–10699. doi: 10.1039/C9TC03464A
- Jin, L., Zhang, X., He, T., Meng, W., Dai, X., and Liu, G. (2020a). Electronic structure, doping effect and topological signature in realistic intermetallics  $Li_{3-x}Na_xM$  ( $x = 3, 2, 1, 0$ ;  $M = N, P, As, Sb, Bi$ ). *Phys. Chem. Chem. Phys.* 22, 5847–5854. doi: 10.1039/C9CP06033B
- Jin, L., Zhang, X., He, T., Meng, W., Dai, X., and Liu, G. (2020b). Ferromagnetic two-dimensional metal-chlorides  $MCl$  ( $M = Sc, Y, and La$ ) candidates for Weyl nodal line semimetals with small spin-orbit coupling gaps. *Appl. Surface Sci.* 520:146376. doi: 10.1016/j.apsusc.2020.146376
- Jin, L., Zhang, X., Liu, Y., Dai, X., Shen, X., Wang, L., et al. (2020c). Two-dimensional Weyl nodal-line semimetal in a  $d^0$  ferromagnetic  $K_2N$  monolayer with a high Curie temperature. *Phys. Rev. B* 102:125118. doi: 10.1103/PhysRevB.102.125118
- Jin, L., Zhang, X. M., Dai, X. F., Wang, L. Y., Liu, H. Y., and Liu, G. D. (2019a). Screening topological materials with a  $CsCl$ -type structure in crystallographic databases. *IUCrJ* 6, 688–694. doi: 10.1107/S2052252519007383
- Jing, Y., and Heine, T. (2018). Two-dimensional kagome lattices made of hetero triangulenes are Dirac semimetals or single-band semiconductors. *J. Am. Chem. Soc.* 141, 743–747. doi: 10.1021/jacs.8b09900
- Kambe, T., Sakamoto, R., Kusamoto, T., Pal, T., Fukui, N., Hoshiko, K., et al. (2014). Redox control and high conductivity of nickel bis (dithiolene) complex  $\pi$ -nanosheet: a potential organic two-dimensional topological insulator. *J. Am. Chem. Soc.* 136, 14357–14360. doi: 10.1021/ja507619d
- Khoury, J. F., Rettie, A. J., Khan, M. A., Ghimire, N. J., Robredo, I., Pfluger, J. E., et al. (2019). A new three-dimensional subsulfide  $Ir_2In_8S$  with Dirac semimetal behavior. *J. Am. Chem. Soc.* 141, 19130–19137. doi: 10.1021/jacs.9b10147
- Klemenz, S., Hay, A. K., Teicher, S. M., Topp, A., Cano, J., and Schoop, L. M. (2020). The role of delocalized chemical bonding in square-net-based topological semimetals. *J. Am. Chem. Soc.* 142, 6350–6359. doi: 10.1021/jacs.0c01227
- Kong, D., and Cui, Y. (2011). Opportunities in chemistry and materials science for topological insulators and their nanostructures. *Nat. Chem.* 3, 845–849. doi: 10.1038/nchem.1171
- Kresse, G., and Furthmüller, J. (1996). Efficient iterative schemes for ab initio total-energy calculations using a plane-wave basis set. *Phys. Rev. B* 54:11169. doi: 10.1103/PhysRevB.54.11169
- Li, H., Cao, J., Zheng, W., Chen, Y., Wu, D., Dang, W., et al. (2012). Controlled synthesis of topological insulator nanoplate arrays on mica. *J. Am. Chem. Soc.* 134, 6132–6135. doi: 10.1021/ja3021395
- Li, Y., and Xia, J. (2020). Cubic hafnium nitride: a novel topological semimetal hosting a 0-Dimensional (0-D) triple nodal point and a 1-D topological nodal ring. *Front. Chem.* 8:727. doi: 10.3389/fchem.2020.00727
- Li, Y., Xia, J., Khenata, R., and Kuang, M. (2020a). Insight into the topological nodal line metal  $YB_2$  with large linear energy range: a first-principles study. *Materials* 13:3841. doi: 10.3390/ma13173841
- Li, Y., Xia, J., and Srivastava, V. (2020b). The tetragonal monoxide of platinum: a new platform for investigating nodal-line and nodal-point semimetallic behavior. *Front. Chem.* 8:704. doi: 10.3389/fchem.2020.00704
- Lin, C. L., Arafune, R., Liu, R. Y., Yoshimura, M., Feng, B., Kawahara, K., et al. (2017). Visualizing type-II Weyl points in tungsten ditelluride by quasiparticle interference. *ACS Nano* 11, 11459–11465. doi: 10.1021/acsnano.7b06179
- Liu, G., Jin, L., Dai, X., Chen, G., and Zhang, X. (2018a). Topological phase with a critical-type nodal line state in intermetallic  $CaPd$ . *Phys. Rev. B* 98:075157. doi: 10.1103/PhysRevB.98.075157
- Liu, G. D., Zhai, X., Meng, H. Y., Lin, Q., Huang, Y., Zhao, C. J., et al. (2018b). Dirac semimetals based tunable narrowband absorber at terahertz frequencies. *Opt. Exp.* 26, 11471–11480. doi: 10.1364/OE.26.011471
- Liu, J., Cheng, L., Zhao, D., Chen, X., Sun, H., Zhu, J. X., et al. (2020). Quenching of the relaxation pathway in the Weyl semimetal  $TaAs$ . *Phys. Rev. B* 102:064307. doi: 10.1103/PhysRevB.102.064307
- Meng, L., Li, Y., Wu, J., Zhao, L., and Zhong, J. (2020). A type of novel Weyl semimetal candidate: layered transition metal monochalcogenides  $Mo_2XY$  ( $X, Y = S, Se, Te, X \neq Y$ ). *Nanoscale* 12, 4602–4611. doi: 10.1039/C9NR09123H
- Meng, W., Zhang, X., Dai, X., and Liu, G. (2020a).  $IrSi$  as a superior electronic material with novel topological properties and nice compatibility with semiconductor  $Si$ . *Phys. Status Solidi–Rapid Res. Lett.* 14:2000178. doi: 10.1002/psrr.202000178
- Meng, W., Zhang, X., He, T., Jin, L., Dai, X., Liu, Y., et al. (2020b). Ternary compound  $HfCuP$ : An excellent Weyl semimetal with the coexistence of type-I and type-II Weyl nodes. *J. Adv. Res.* 24, 523–528. doi: 10.1016/j.jare.2020.05.026
- Murnaghan, F. D. (1944). The compressibility of media under extreme pressures. *Proc. Natl. Acad. Sci. U.S.A.* 30:244. doi: 10.1073/pnas.30.9.244
- Peng, B., Zhang, H., Shao, H., Lu, H., Zhang, D. W., and Zhu, H. (2016). High thermoelectric performance of Weyl semimetal  $TaAs$ . *Nano Energy* 30, 225–234. doi: 10.1016/j.nanoen.2016.10.016
- Peng, H., Dang, W., Cao, J., Chen, Y., Wu, D., Zheng, W., et al. (2012). Topological insulator nanostructures for near-infrared transparent flexible electrodes. *Nat. Chem.* 4, 281–286. doi: 10.1038/nchem.1277
- Perdew, J. P., Burke, K., and Ernzerhof, M. (1996). Generalized gradient approximation made simple. *Phys. Rev. Lett.* 77:3865. doi: 10.1103/PhysRevLett.77.3865
- Perdew, J. P., Burke, K., and Ernzerhof, M. (1998). Perdew, burke, and ernzerhof reply. *Phys. Rev. Lett.* 80:891. doi: 10.1103/PhysRevLett.80.891

- Rasche, B., Isaeva, A., Ruck, M., Borisenko, S., Zabolotnyy, V., Büchner, B., et al. (2013). Stacked topological insulator built from bismuth-based graphene sheet analogues. *Nat. Mater.* 12, 422–425. doi: 10.1038/nmat3570
- Schoop, L. M., Pielhofer, F., and Lotsch, B. V. (2018). Chemical principles of topological semimetals. *Chem. Mater.* 30, 3155–3176. doi: 10.1021/acs.chemmater.7b05133
- Sheng, X. L., Yu, Z. M., Yu, R., Weng, H., and Yang, S. (2017). A d orbital topological insulator and semimetal in the antiferromagnetic Cu<sub>2</sub>S family: contrasting spin helicities, nodal box, and hybrid surface states. *J. Phys. Chem. Lett.* 8, 3506–3511. doi: 10.1021/acs.jpcclett.7b01390
- Tang, F., Po, H. C., Vishwanath, A., and Wan, X. (2019). Comprehensive search for topological materials using symmetry indicators. *Nature* 566, 486–489. doi: 10.1038/s41586-019-0937-5
- Walsh, L. A., Smyth, C. M., Barton, A. T., Wang, Q., Che, Z., Yue, R., et al. (2017). Interface chemistry of contact metals and ferromagnets on the topological insulator Bi<sub>2</sub>Se<sub>3</sub>. *J. Phys. Chem. C* 121, 23551–23563. doi: 10.1021/acs.jpcc.7b08480
- Wang, J. T., Nie, S., Weng, H., Kawazoe, Y., and Chen, C. (2018). Topological nodal-net semimetal in a graphene network structure. *Phys. Rev. Lett.* 120:026402. doi: 10.1103/PhysRevLett.120.026402
- Wang, S. S., Wu, W. K., and Yang, S. Y. (2019). Progress on topological nodal line and nodal surface. *Acta Phys. Sinica* 68:227101. doi: 10.7498/aps.68.20191538
- Wang, X., Cheng, Z., Zhang, G., Wang, B., Wang, X. L., and Chen, H. (2020a). Rich novel zero-dimensional (0D), 1D, and 2D topological elements predicted in the P6<sub>3</sub>/m type ternary boride HfBr<sub>3</sub>B<sub>4</sub>. *Nanoscale* 12, 8314–8319. doi: 10.1039/D0NR00635A
- Wang, X., Ding, G., Cheng, Z., Surucu, G., Wang, X. L., and Yang, T. (2020b). Novel topological nodal lines and exotic drum-head-like surface states in synthesized CsCl-type binary alloy TiOs. *J. Adv. Res.* 22, 137–144. doi: 10.1016/j.jare.2019.12.001
- Wang, X., Ding, G., Cheng, Z., Surucu, G., Wang, X. L., and Yang, T. (2020c). Rich topological nodal line bulk states together with drum-head-like surface states in NaAlGe with anti-PbFCl type structure. *J. Adv. Res.* 23, 95–100. doi: 10.1016/j.jare.2020.01.017
- Wang, X., Ding, G., Cheng, Z., Wang, X. L., Zhang, G., and Yang, T. (2020d). Intersecting nodal rings in orthorhombic-type BaLi<sub>2</sub>Sn compound. *J. Mater. Chem. C* 8, 5461–5466. doi: 10.1039/D0TC00504E
- Wang, X., Ding, G., Khandy, S. A., Cheng, Z., Zhang, G., Wang, X. L., et al. (2020e). Unique topological nodal line states and associated exceptional thermoelectric power factor platform in Nb<sub>3</sub>GeTe<sub>6</sub> monolayer and bulk. *Nanoscale* 12, 16910–16916. doi: 10.1039/D0NR03704D
- Wang, X., Zhou, F., and Chen, H. (2020f). Organic-inorganic hybrid coordination polymer C<sub>3</sub>H<sub>9</sub>CdCl<sub>3</sub>N co-exhibiting superior Dirac point and nodal surface states. *Results Phys.* 17:103159. doi: 10.1016/j.rinp.2020.103159
- Wang, Z. F., Su, N., and Liu, F. (2013). Prediction of a two-dimensional organic topological insulator. *Nano Lett.* 13, 2842–2845. doi: 10.1021/nl401147u
- Wu, M., Han, Y., Bouhemadou, A., Cheng, Z., Khenata, R., Kuang, M., et al. (2019). Site preference and tetragonal distortion in palladium-rich Heusler alloys. *IUCr* 6, 218–225. doi: 10.1107/S2052252518017578
- Wu, W., Liu, Y., Li, S., Zhong, C., Yu, Z. M., Sheng, X. L., et al. (2018). Nodal surface semimetals: theory and material realization. *Phys. Rev. B* 97:115125. doi: 10.1103/PhysRevB.97.115125
- Xu, Q., Yu, R., Fang, Z., Dai, X., and Weng, H. (2017). Topological nodal line semimetals in the CaP<sub>3</sub> family of materials. *Phys. Rev. B* 95:045136. doi: 10.1103/PhysRevB.95.045136
- Xu, S. G., Chen, Z. J., Zhao, Y. J., Zhang, X., Xu, H., and Yang, X. B. (2020). Realizing graphene-like Dirac cones in triangular boron sheets by chemical functionalization. *J. Mater. Chem. C* 8, 2798–2805. doi: 10.1039/C9TC06464H
- Yan, Z., Bi, R., Shen, H., Lu, L., Zhang, S. C., and Wang, Z. (2017). Nodal-link semimetals. *Phys. Rev. B* 96:041103. doi: 10.1103/PhysRevB.96.041103
- Zeugner, A., Nietschke, F., Wolter, A. U., Gaß, S., Vidal, R. C., Peixoto, T. R., et al. (2019). Chemical aspects of the candidate antiferromagnetic topological insulator MnBi<sub>2</sub>Te<sub>4</sub>. *Chem. Mater.* 31, 2795–2806. doi: 10.1021/acs.chemmater.8b05017
- Zhang, G., Qin, H., Chen, J., He, X., Lu, L., Li, Y., et al. (2011). Growth of topological insulator Bi<sub>2</sub>Se<sub>3</sub> thin films on SrTiO<sub>3</sub> with large tunability in chemical potential. *Adv. Funct. Mater.* 21, 2351–2355. doi: 10.1002/adfm.201002667
- Zhang, M., Yang, Z., and Wang, G. (2018c). Coexistence of Type-I and Type-II Weyl points in the Weyl-semimetal OsC<sub>2</sub>. *J. Phys. Chem. C* 122, 3533–3538. doi: 10.1021/acs.jpcc.8b00920
- Zhang, X., Fu, B., Jin, L., Dai, X., Liu, G., and Yao, Y. (2019). Topological nodal line electrides: realization of an ideal nodal line state nearly immune from spin-orbit coupling. *J. Phys. Chem. C* 123, 25871–25876. doi: 10.1021/acs.jpcc.9b08446
- Zhang, X., Guo, R., Jin, L., Dai, X., and Liu, G. (2018a). Intermetallic Ca<sub>3</sub>Pb: a topological zero-dimensional electride material. *J. Mater. Chem. C* 6, 575–581. doi: 10.1039/C7TC04989G
- Zhang, X., Liu, Q., Xu, Q., Dai, X., and Zunger, A. (2018b). Topological insulators versus topological Dirac semimetals in honeycomb compounds. *J. Am. Chem. Soc.* 140, 13687–13694. doi: 10.1021/jacs.8b06652
- Zhao, B., Guo, C., Garcia, C. A., Narang, P., and Fan, S. (2020). Axion-field-enabled nonreciprocal thermal radiation in Weyl semimetals. *Nano Lett.* 20, 1923–1927. doi: 10.1021/acs.nanolett.9b05179
- Zhao, X., and Ma, F. (2020). Hexagonal wurtzite MnO in ferromagnetic state: A magnetic topological spin-gapless Weyl semimetal. *Phys. Lett. A* 384:126494. doi: 10.1016/j.physleta.2020.126494
- Zhao, Z., Zhang, Z., and Guo, W. (2020). A family of all sp<sup>2</sup>-bonded carbon allotropes of topological semimetals with strain-robust nodal-lines. *J. Mater. Chem. C* 8, 1548–1555. doi: 10.1039/C9TC05470G
- Zhong, C., Chen, Y., Xie, Y., Sun, Y. Y., and Zhang, S. (2017). Semi-Dirac semimetal in silicene oxide. *Phys. Chem. Chem. Phys.* 19, 3820–3825. doi: 10.1039/C6CP08439G
- Zhong, C., Chen, Y., Xie, Y., Yang, S. A., Cohen, M. L., and Zhang, S. B. (2016). Towards three-dimensional Weyl-surface semimetals in graphene networks. *Nanoscale* 8, 7232–7239. doi: 10.1039/C6NR00882H
- Zhou, F., Ding, G., Cheng, Z., Surucu, G., Chen, H., and Wang, X. (2020). Pnma metal hydride system LiBH: a superior topological semimetal with the coexistence of twofold and quadruple degenerate topological nodal lines. *J. Phys.* 32:365502. doi: 10.1088/1361-648X/ab8f5d
- Zhou, P., Ma, Z. S., and Sun, L. Z. (2018). Coexistence of open and closed type nodal line topological semimetals in two dimensional B2C. *J. Mater. Chem. C* 6, 1206–1214. doi: 10.1039/C7TC05095J
- Zhou, Y., Zhao, Y. Q., Zeng, Z. Y., Chen, X. R., and Geng, H. Y. (2019). Anisotropic thermoelectric properties of Weyl semimetal NbX (X = P and As) a potential thermoelectric material. *Phys. Chem. Chem. Phys.* 21, 15167–15176. doi: 10.1039/C9CP02020A

**Conflict of Interest:** The authors declare that the research was conducted in the absence of any commercial or financial relationships that could be construed as a potential conflict of interest.

Copyright © 2020 Xu, Xi and Gao. This is an open-access article distributed under the terms of the Creative Commons Attribution License (CC BY). The use, distribution or reproduction in other forums is permitted, provided the original author(s) and the copyright owner(s) are credited and that the original publication in this journal is cited, in accordance with accepted academic practice. No use, distribution or reproduction is permitted which does not comply with these terms.